Richard Volpe

Jet Propulsion Laboratory
California Institute of Technology
Pasadena, California 91109, USA
volpe@jpl.nasa.gov

Navigation Results from Desert Field Tests of the *Rocky 7* Mars Rover Prototype

Abstract

Upcoming missions to the surface of Mars will use mobile robots to traverse long distances from the landing site. To prepare for these missions, the prototype rover, Rocky 7, *has been tested in desert field trials conducted with a team of planetary scientists. While several new capabilities have been demonstrated, foremost among these was sun-sensor-based traversal of natural terrain totaling a distance of 1 km. This paper describes navigation results obtained in the field tests, where cross-track error was only 6% of the distance traveled. Comparison with previous results of other planetary rover systems shows this to be a significant improvement. Methods for further improvement are also discussed.*

KEY WORDS—field robotics, planetary rovers, mobile robot navigation, localization

1. Introduction

In 1997, NASA revisited the planet Mars for the first time in 20 years. The *Pathfinder*[1] lander contained the mobile robot, *Sojourner*, a 12-kg, 6-wheeled rover that ventured out from the lander, taking pictures and positioning a science instrument against designated soil and rocks (Matijevic et al. 1997a, 1997b). Based on previous rover prototypes (Gat et al. 1994), *Sojourner* was designed to demonstrate the viability of mobile robot exploration of Mars.

Current plans are to build on this successful test of a planetary rover with longer-range traversals across Mars beginning in 2003. Therefore, we have been investigating next-generation prototype rovers with more manipulation, mobility, autonomy, and general functionality (Volpe et al. 1996).

This paper describes our prototype rover, *Rocky 7*, and its successful desert field trials of the long-range mission scenario.[2] Among the important new capabilities demonstrated are the following: accurate sun-sensor-based navigation over long distances, operator control using rover-centric imagery, traversal contextualization from panoramic mosaics and nested descent imagery, and remote autonomous scientific exploration of an extended geologic area. Specific details are provided on the performance of navigation using the sun's position in the sky, the local vertical, and the time of day to calculate heading and control the rover's direction of travel.

This paper is organized as follows: Section 2 describes many of the features of our test vehicle, *Rocky 7*, and is followed by a description of its navigation command and control strategies in Section 3. Section 4 provides an overview of the desert-field-test objectives and implementation. Experimental results are presented and analyzed in Section 5, and the indicated areas and methods for improving performance are discussed in Section 6.

2. *Rocky 7*: An Overview

Figure 1 shows the *Rocky 7* Mars rover research prototype. Whereas *Sojourner* employed technology demonstrated in previous prototypes (e.g., *Rocky 3* and *Rocky 4*), *Rocky 7* was designed to advance rover technology for future missions, such as the upcoming Mars Surveyor Rover Mission.[3] Among these rover technologies are reduced actuator mobility, appendages and algorithms for sampling and periscopic viewing, improved actuation and sensing, computationally intensive sensor processing, and a contemporary computing environment (Volpe et al. 1997a, 1997b, 1998). Also required for terrestrial tests were well-designed power and thermal systems. Each of these is discussed below.

2.1. Mobility and Manipulation

Rocky 7 is slightly larger and heavier than *Sojourner*, being $60 \times 40 \times 35\text{cm}^3$ and 15.5 kg. Like *Sojourner*, *Rocky 7*

The International Journal of Robotics Research
Vol. 18, No. 7, July 1999, pp. 669-683,

1. See the World Wide Web at http://mpfwww.jpl.nasa.gov/.

2. See the World Wide Web at http://robotics.jpl.nasa.gov/tasks/lrsr/.

3. See the World Wide Web at http://mars.jpl.nasa.gov/.

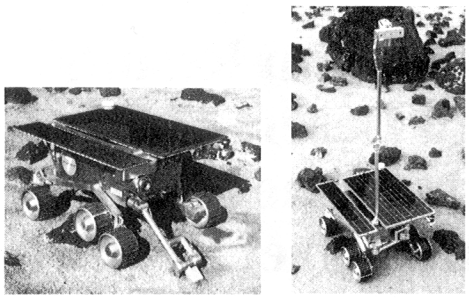

(a) (b)

Fig. 1. The *Rocky 7* rover with (a) arm deployed, or (b) mast up.

employs a *rocker-bogie* six-wheel configuration (Bickler 1992). However, unlike its predecessors with four-corner steering, *Rocky 7* only has steering capability on two corners, driving like a car or forklift. Also, the wheels on each bogie have been moved close together. While not greatly reducing its step-climbing capability of greater than 1.2 wheel diameters, this configuration creates the possibility of mechanically or electrically controlling these two wheels together. In this way, the number of degrees of freedom (DoF) for mobility has been reduced from 10 to 6. The cost of this change is an inability to turn in place about the center of the vehicle, as with four-corner steering. Instead, the nominal rotation axis for *Rocky 7* is located midway between the double-wheel pairs. (Tank steering can be used to approximate turn-in-place operations, but the extensive wheel slippage corrupts odometer information, and would cause the vehicle to sink into soft soils like those expected on Mars.)

The four DoFs saved with the new wheel configuration have been used for a manipulator that can sample soil or rocks, and point or bury science instruments, as shown in Figure 1a. This small arm has a 2-DoF shoulder that can store it across the front of the chassis, reach down to 10 cm below the surface, or move in a conical fashion in front of the vehicle to point an integrated spectrometer. The end effector of the arm has two independently drivable scoops, which can rotate continuously. In this way, they can be positioned as a clamshell to scoop and store soil samples, or back to back to form a parallel jaw gripper with interleaved tongs allowing rock and cylindrical instrument grasping. Also, when rotated together through 360°, they deploy a white target stored in the fork of the end effector. This target is used for calibrating a built-in spectrometer (Volpe et al. 1997b).

A second, longer, 3-DoF manipulator deploys through a slot in the solar panel, and is referred to as "the mast," as shown in Figure 1b. It carries an integrated sensor package which has stereo cameras with counter-rotating filter wheels, and an interchangeable instrument canister. The primary function of the mast is to extend to a height of 1.4 m from ground level and rotate 360° to provide panoramic imagery. It can also look down at the surrounding terrain or the rover itself, enabling visual self-inspection from all directions. This dexterity also enables the positioning of the instrument canister on nearby rocks and soil. Typically the canister is outfitted with a gimbaled close-focus camera, but mast payload specifications (0.5 kg) are designed to allow the replacement of the close-up imager with another science instrument, such as the Mössbauer spectrometer used in the desert tests.[4] Finally, when stowed, the arm does not cast a shadow on the solar panel, block the navigation cameras, or impede the motion of the rocker-bogies.

2.2. Actuation and Sensing

Rocky 7's manipulators and steering wheels use a specially developed modular joint design (Volpe et al. 1998). Two features of this joint that are of particular value to robotics applications are its hollow axis and backdriveability. The former is valuable because robots typically employ serial chains of actuators, and the hollow axis allows wiring to pass through each joint without service loops. It has also proven useful on *Rocky 7* as an optical pathway for the spectrometer integrated into the shorter manipulator. The latter is valuable since backdriveable joints accommodate reaction forces during contact operations, enabling better sensing and control. Also, from a practical standpoint, during development joints may be manually moved when unpowered.

To control the motors in all actuators of the rover, we have developed a customized independent joint control system. While similar capability can be obtained from off-the-shelf hardware, limitations in mass, power, and volume required the development of custom electronics. Each motor is servoed with a proportional-integral-derivative (PID) control loop that relies on the input of quadrature encoder measurements of joint position, and creates a pulse-width-modulated (PWM) output for motor current. This type of motor control allows accurate positioning of the appendages, and variable speed trajectory profiles for slipless wheel acceleration. Motor current is also measured for use in certain applications, such as contact detection while digging.

Beyond the encoders and current sensing, *Rocky 7* has a full suite of navigation sensors. The configuration of the rocker-bogie suspension is measured with potentiometers, and the tilt of the chassis is obtained with three accelerometers. A quartz rate sensor can measure the rate of rotation of the vehicle about its vertical axis, but this measurement must be integrated to provide heading, making it subject to drift as bias error is integrated with the rate signal. The amount of drift is proportional to the total time of integration, and therefore the distance traveled divided by the speed. Faster speeds can reduce the error, but they may also increase vehicle vibration on rough terrain, another source of noise and drift. Optimal speeds are not known at this time. For all of these reasons, absolute heading sensors are a better solution.

On Earth, the magnetic compass is the most common absolute heading device. However, use of a compass is not

4. See the World Wide Web at http://astrosun.tn.cornell.edu/athena/mossbauer.html.

legitimate for our tests, since Mars has a negligible magnetic field. Star tracking is not an option because it will not provide heading during the daytime, and it typically requires narrow field-of-view imaging made difficult by rover motion over rough terrain (Cozman and Krotkov 1997). Horizon-feature tracking is computationally intensive, and will not work in featureless terrains such as the *Viking Lander II* site on Mars (Cozman and Krotkov 1995).

Therefore, to provide a reliable measurement of the vehicle heading, we have employed a wide field-of-view sun sensor. This sensor is rigidly attached to the rover, facing upward. It projects an image of the sky onto a two-dimensional analog position-sensing device (PSD), which puts out signals proportional to the centroid of the intensity image (Fraden 1993). Used in conjunction with the accelerometer readings and an onboard clock, it enables absolute vehicle heading to be calculated (Wertz 1980).

Since the sun sensor is essentially a camera, a CCD could be used instead of the PSD, and image processing could be employed to extract the sun position. However, the PSD-based sensor employed on *Rocky 7* is attractive for its fast rate of update and minimal computational overhead (Price et al. 1996). This simplicity and speed come at the cost of increased complexity of calibration, and slight miscalibration did lead to test errors, which are discussed in Section 5.1. (Subsequent recalibration has been performed, and the sensor is being used in ongoing improvements in rover-position estimation filters, which rely on the fast update rate provided by its analog design.)

Although not employed for sun sensing, black-and-white CCD cameras are used extensively on *Rocky 7*, for hazard avoidance, navigation telemetry, and science data. Images from sets of these cameras are captured simultaneously as stereo pairs. Mast imagery is typically returned to the rover operators as panoramic mosaics for use in specifying rover traversals. Body-mounted hazard-avoidance images are typically processed onboard to provide depth maps of the environment, and then automatically analyzed for abrupt changes in height or high-centering hazards (Matthies and Grandjean 1994; Volpe et al. 1997b). Impassable regions are specified to the navigation algorithm through a fuzzy classification of the region position: left, right, or center. The central region is defined as the width of the vehicle extending out to 50 cm. The left and right regions are from either side of the central region to the edge of the field of view. Navigation based on this classification is reviewed in Section 3.

2.3. Computing

To support computationally intensive processing such as stereo vision algorithms, and to provide a contemporary software-development environment, *Rocky 7* has a 32-bit computer running a commercial hard-real-time operating system (Wind River Systems' VxWorks). *Rocky 7*'s software architecture is based on the framework provided by Real Time Innovation's Control Shell (Schneider, Chen, and Pardo-Castellote 1994). Control Shell facilitates the creation of C++ software modules, which are connected into asynchronous finite-state machines and synchronous data-flow control loops. In *Rocky 7*, asynchronous activities are initiated by a queue of operator commands. Onboard the rover, these commands cause state transitions in one of several state machines for navigation, vision, and manipulation. State-machine transitions are often used to begin the execution of synchronous processes which perform monitoring and control of the rover's subsystems.

2.4. Power and Thermal Issues

Power and thermal issues for *Rocky 7* are unique to its application as an Earth research test vehicle. Power consumption has been kept in check, but not at the cost incurred on typical space missions, where custom design is the rule. *Rocky 7*'s commercial off-the-shelf (COTS) electronics were selected to provide needed functionality while minimizing power consumption, temperature tolerance, mass, and volume. The resulting system consumes approximately 50 W while driving, and is powered by rechargeable NiCad batteries and a 0.25m^2 solar panel. During typical activities for the rover, batteries must be replaced every 1.5 hr.

Thermal concerns on Earth are governed by the need to keep components cool, whereas on Mars they must be kept warm. To remove heat from the chassis containing the electronics, a bank of fans forces air under the solar panel. All electronic components in the vehicle are rated to at least 60°C. During the desert-field tests described in this report, internal rover temperatures were held within their limits even as ambient air temperature reached 45°C.

3. *Rocky 7* Navigation

After the completion of *Rocky 7*'s construction and baseline programming, a series of increasingly lengthy demonstrations were conducted in the JPL MarsYard outdoor test area and the Mojave desert. Contained, herein, are the results of the last of these tests, a simulated mission performed at Lavic Lake lava flow and dry lake bed on the Twenty Nine Palms Marine Corps Base (Arvidson et al. 1998). During this simulation, *Rocky 7* traversed more than 1 km across four distinct terrains, while commanded remotely by a team of scientists and engineers.

The strategy for a simulated exploration of Mars, as with a real mission, requires the rover to simply go where commanded, within the limits allowed by the onboard safety system (Whittaker et al. 1997). This ability depends on reliable techniques for operator interfacing, mobility, hazard detection, piloting, and position estimation of the rover.

Rocky 7's operator interface is the *Web Interface for Telescience (WITS)* (Backes, Tso, and Tharp 1998). Through it, an

operator is provided with panoramic stereo images taken from *Rocky 7*'s deployable mast, or with aerial images obtained during an emulation of the lander's descent (obtained by helicopter). From this imagery, samples of which are shown in Figures 2 and 3, waypoints and science targets are selected and incorporated in a sequential list sent to the rover.

The rover interprets each waypoint as a goal to which it must navigate while avoiding obstacles. Stereo images of the terrain are processed onboard the rover, and some terrain features are interpreted as obstacles (Matthies and Grandjean 1994). Based on the location of obstacles and the goal with respect to the rover, very simple reactive rules are used to decide its piecewise motion (Volpe et al. 1996; Gat et al. 1994; Brooks 1986). That is, the rover either turns in place by 0.5 rad, or moves forward in 0.25 m path segments that are straight or in an arc toward the goal. Then the entire procedure is repeated.

The performance of this sequence of activities depends heavily on the accuracy of the position estimate of the rover—globally, locally, and incrementally. Position estimation of the rover is comprised of down-track and cross-track estimation of position as the rover traverses. First-order estimates of the down-track position are obtained directly from wheel odometry. However, the accuracy of the position estimate is largely dependent on knowledge of heading, because small heading errors can develop into large cross-track position errors during extended traversals. As described in Section 2.2, sun sensing has been employed on *Rocky 7* to provide a useful heading estimate (Volpe 1998).

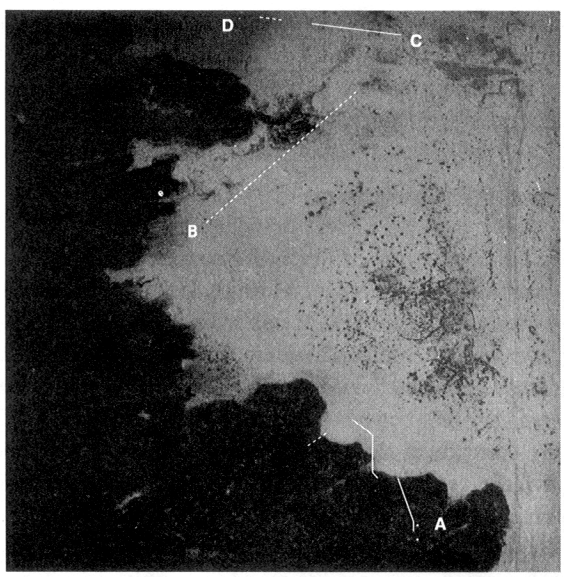

Fig. 2. Imagery of the Lavic Lake site at 862 m above ground level, taken by helicopter during an emulated lander descent. Letters indicate the location of prepositioned ground targets; solid lines indicate the rover traverses that are discussed in detail; and dashed lines indicate other rover traverses. The direct distance from A to D is approximately 1 km.

4. Field-Test Objectives and Implementation

The selected site for the field tests was Lavic Lake, a dry lake bed bordered by a lava flow and a geologic fault line, and pock-marked from Marine bombing practice. Figure 2 is an aerial view of the test site on the southwestern edge of the lake bed. This location was chosen specifically for these tests by Ray Arvidson, Chair of Planetary Sciences at Washington University, who led the science team's efforts for this demonstration in preparation for his role as Science Operations Lead in the upcoming Mars Surveyor 2003 Rover Mission.

Located on a Marine Corps base in the Mojave desert, Lavic Lake was also logistically attractive. First, it is only a 3 hr drive from JPL, minimizing transportation difficulties. Second, the use of off-road vehicles (including the rover itself), and a radioactive source for the Mössbauer spectrometer, were permitted by the Marines. Such permission was not readily available from the National Park Service or Bureau of Land Management, which have jurisdiction over most desert lands in California. Third, Marine bombing practice has left many portions of Lavic Lake with craters, providing a nice Mars analog terrain.

For the engineering team, these tests were designed to provide a demonstration of the system performing long-distance traversals and remote science operations without the aid of a lander. For the science team, such a demonstration would give a preview of rover capabilities and limitations to be expected for upcoming Mars missions. In both cases, it was assumed that there would be some validation and some recalibration of expectations and understanding.

In preparation for the tests, four geologically distinct science sites were chosen within the Lavic Lake area: a lava flow with desert pavement, undisturbed playa, cratered playa, and an alluvial fan. Each of these sites was imaged by helicopter in a nested sequence that emulated planned lander-descent images for upcoming missions. Figure 2 shows one image from these sequences that captures all four regions.

The operations center for the tests was located in a trailer parked close to point B. In addition to the emulated descent imagery, the rover operator and scientists made all mission decisions based on information sent back from *Rocky 7* in the form of images and other telemetry. A complete log of this information is available over the Internet.[5]

In addition to the telemetry used for mission planning, two other forms of data were collected. First, a complete log of the rover's onboard command sequencing was captured, as well as rover position estimates at each navigation step. Second, approximately every 3 m of traverse, the rover position was

5. See the World Wide Web at http://wundow.wustl.edu/rocky7/.

Fig. 3. Panoramic mosaic taken by the mast cameras of *Rocky 7* from the beginning of the traverse from point A in Figure 2. The center of the mosaic is facing north. The large white patch, visible in both views, is a ground target used for guiding the aerial imaging.

marked and the time noted. The marked locations were later measured with surveying equipment. The results of these measurements are presented in the next section.

5. Experimental Results

This section presents the rover traverse results during the three segments shown by solid lines in Figure 2. The first segment is closest to the bottom of the aerial view and point A, and is referred to as the "Sunshine Flow Traverse." The second segment is just north of this, and is referred to as the "Flow Margin Traverse." The third segment is between points C and D, and is referred to as the "Cratered Playa Traverse." Images in Figure 4 show *Rocky 7* and the terrain from ground level during each of these segments.

Figure 5 shows plan views of measured positions of the rover during the three traverses. All coordinates are in a frame with east as positive x, north as positive y, and the origin located at the base station near point B in Figure 2. The dark line in each plot is the onboard estimate of the rover's position. The label "SPICE" is an acronym of the database in which all of the telemetry was stored: Spacecraft, Planet, and Instrument Configuration matrix and Events (Acton 1996). The squares on each plot are the positions of the rover measured by the Ground Truth Station surveying equipment. The accuracy of these measurements is approximately 20 cm, well below the resolution of the plots. Also shown by solid diamonds are the commanded goal positions, which are generically called waypoints (whether they are intermediate or terminal goal points).

Note that the onboard rover position estimate will typically move directly to a waypoint since the rover always "thinks" it is headed the right way. In those cases where the rover does not reach a waypoint, there has been an error condition which prompted communication with the base station, resulting in a new waypoint being provided. Error conditions during the field test had several sources, and were as simple as inadvertent loss of power due to battery depletion. Also problematic were data dropouts due to lost radio communication during the traverse. These are indicated by missing portions of the dark lines on the plots.

Figure 6 presents the same position data as Figure 5, but plotted explicitly against time from the beginning of the traverse. (Time stamps were not obtained for position measurements at the very end of the Cratered Playa traverse, so the data points have been plotted against the final time.) Time passage due to temporal breaks at meals or end of day have been ignored, but other time passage when the rover was not moving has been included. Typically, the latter was during periods when panoramic images were being taken by the rover or commands were being generated at the base station. These periods appear as flat portions of the plots, and often correspond directly to the positions of the waypoints in Figure 5. A typical cycle of operation involved the rover reaching a commanded position tens of meters away, taking a panorama, and then receiving a new goal based on the new imagery. In a real mission on Mars, each of these cycles would require at least one day, due to limited communication opportunities with the spacecraft.

5.1. Position Error

As described earlier, position error of the rover is comprised of down-track and cross-track error. Figure 7 shows the absolute and relative position errors, as well as their down-track and cross-tack components. Because of the turn in the middle of the Flow Margin traverse, there is a discontinuity in the component values in Figures 7c and 7d. From these plots it is apparent that the error grows linearly with distance traveled, and therefore levels out at a constant percentage of the distance traveled. This percentage is slightly different for the three traverses, and is likely the result of different ground traction or errors in heading estimation, as described below. To further distill this data, the absolute position errors from all traverses have been replotted in Figure 8. A least-squares fit of the points indicates an average relative error of 6%.

5.2. Heading Error

5.2.1. Obstacle-Free Analysis

If the rover is considered to be simply trying to stay in a straight line, the measured position error may be used to

(a)

(b)

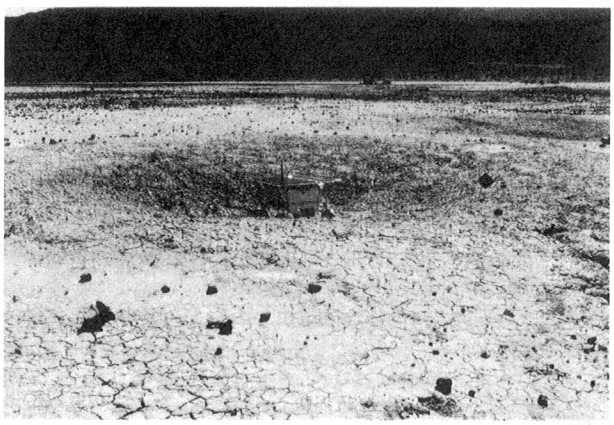

(c)

Fig. 4. Views from ground level of traverse terrain for three segments. (a) Sunshine Flow: Roughest terrain, near beginning of first traverse and A, looking west; (b) Flow Margin: Flow edge at beginning of second traverse, looking north; and (c) Cratered Playa: In shallow crater along third traverse, near C looking northwest.

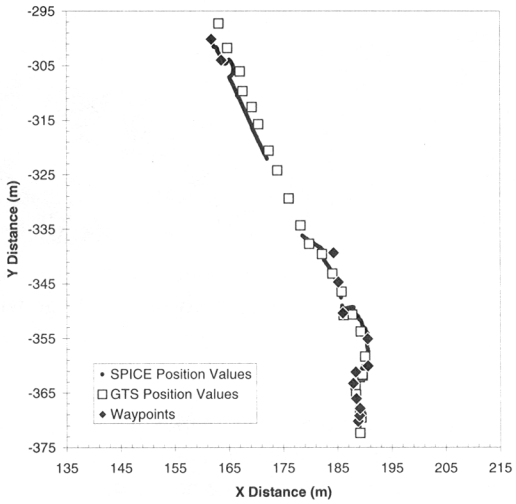

(a) Sunshine flow

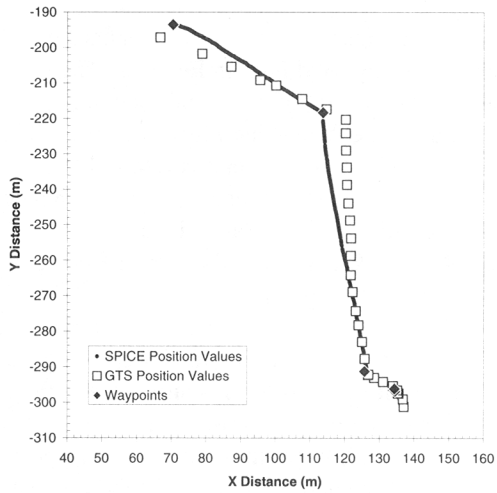

(b) Flow margin

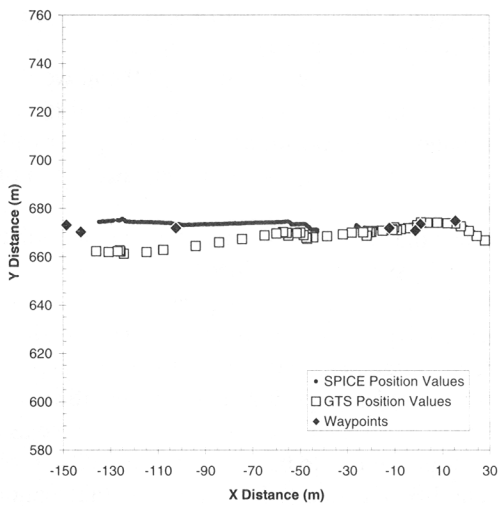

(c) Cratered playa

Fig. 5. Plan view of three rover traverses, showing estimated, measured, and waypoint positions.

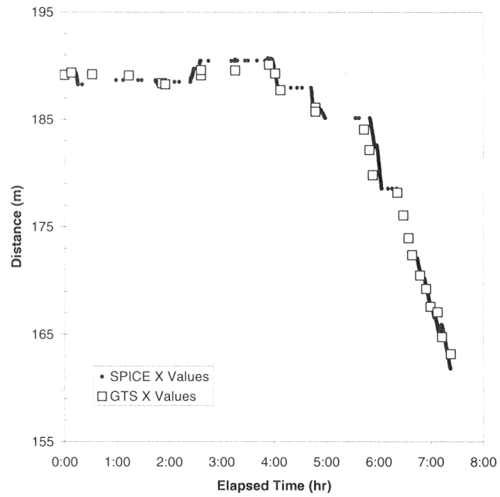

(a) Sunshine flow

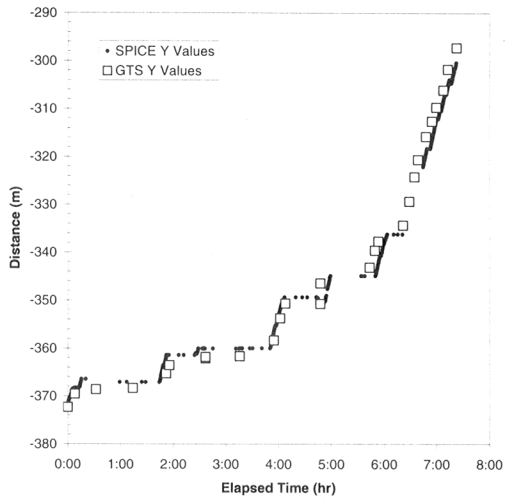

(b) Sunshine flow

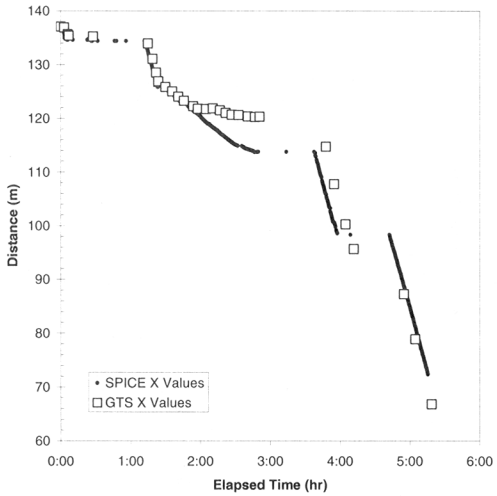

(c) Flow margin

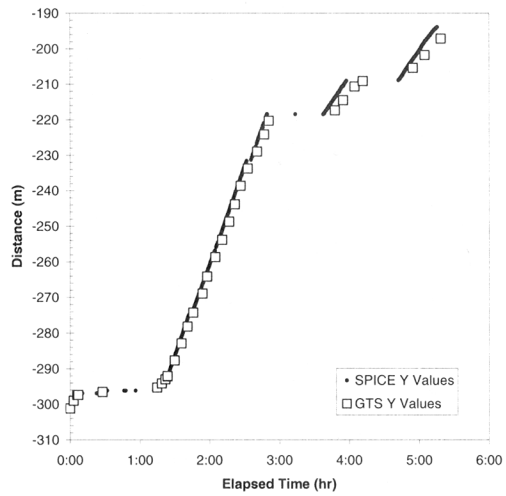

(d) Flow margin

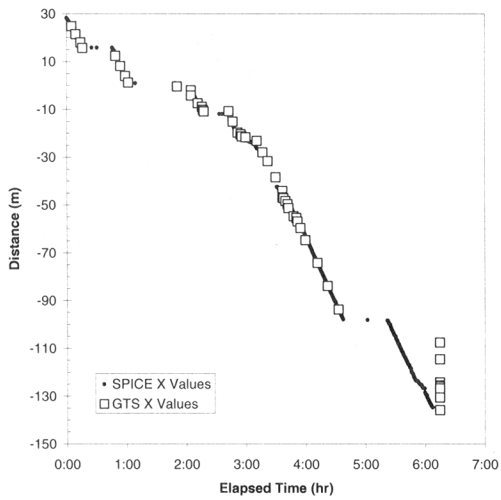

(e) Cratered playa

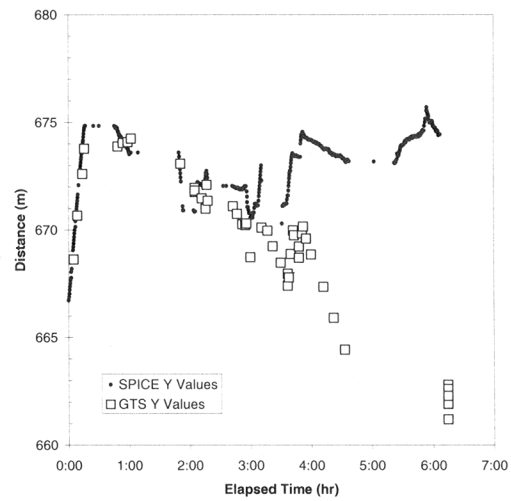

(f) Cratered playa

Fig. 6. Values for x and y over time for the three traverses.

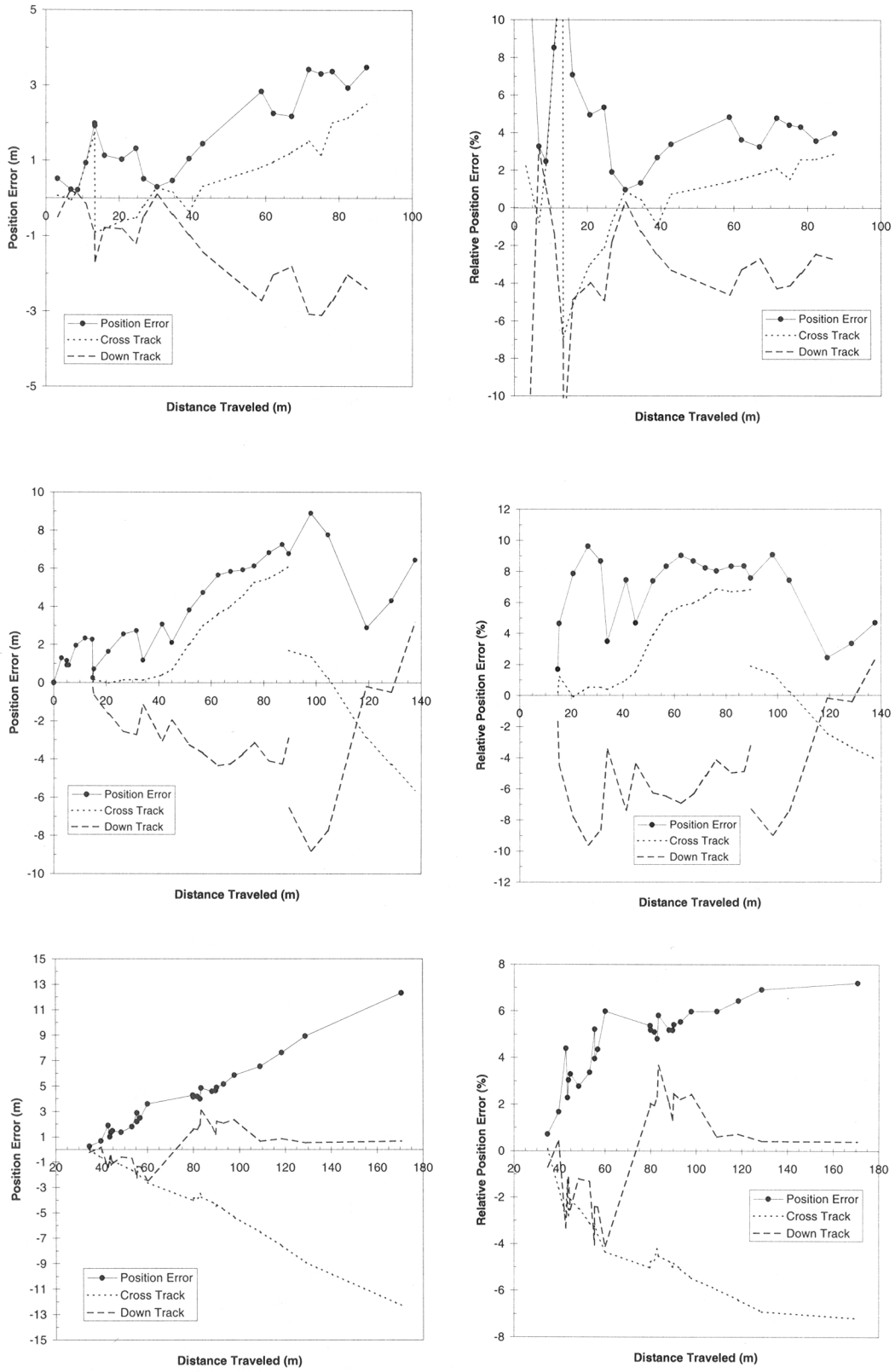

Fig. 7. Absolute and relative errors for rover position during three field-test traversals.

determine the heading error. Since Figure 8 indicates that systematic heading error exists in the measurement for these tests, a simple sensor model assumes an accurate heading angle plus bias:

$$\theta = \theta_0 + e_\theta. \tag{1}$$

For simplicity, we can let $\theta_0 = 0$. Therefore, if the rover speed is v, its (x, y) position will be

$$x = \int_0^t v \cos e_\theta d\tau, \qquad y = \int_0^t v \sin e_\theta d\tau, \tag{2}$$

$$x = vt \cos e_\theta, \qquad y = vt \sin e_\theta. \tag{3}$$

In the absence of bias, the rover would drive straight; that is, with $e_\theta = 0$, $x = vt = d$, and the position error is

$$e_p = \sqrt{(vt \cos e_\theta - vt)^2 + (vt \sin e_\theta)^2} \tag{4}$$

$$= 2d \sin \frac{e_\theta}{2} \tag{5}$$

$$\approx e_\theta d, \tag{6}$$

where the approximation is true for small values of e_θ. It is important to note this result shows that with an absolute heading device like the sun sensor, the relative position error is a constant. From the previous section, $e_p/d = 0.06$ or 3.4°.

5.2.2. *Individual Traversal Results*

For the experimental traversals performed, two issues complicated the situation beyond simply staying in a straight line. First, terrain considerations required that traversals be composed of intermediate waypoints, which sometimes deviated from exactly straight lines. Second, the rover was actively performing hazard avoidance during the traverses, which added to position error and forced time to be spent at headings other than those to the goal.

For these reasons, it is illustrative to look in detail at the heading of the rover during the individual traversals. Figure 9 shows the heading measurements and their distributions for the three traverses. Note that the externally measured heading values, indicated by squares, are very sporadic. This was due to the limited opportunities to measure the orientation of the rover, since it was moving and care was needed to not enter the field of view of the sun sensor or the hazard-detection cameras.

The heading values represented in the figures may be quantified by looking at the statistics of the measurements, shown in Table 1. Greater deviation in the heading is due to more frequent turning of the rover to avoid obstacles or reach intermediate waypoints. This action is typically marked by large changes, as seen in Figure 9a, and is consistent with the rough terrain and numerous waypoints of this traverse. Smaller fluctuations in the heading, as shown in Figure 9c, are often due to other sources such as sun-sensor noise, accelerometer noise, or sun-sensor calibration error (Volpe 1998).

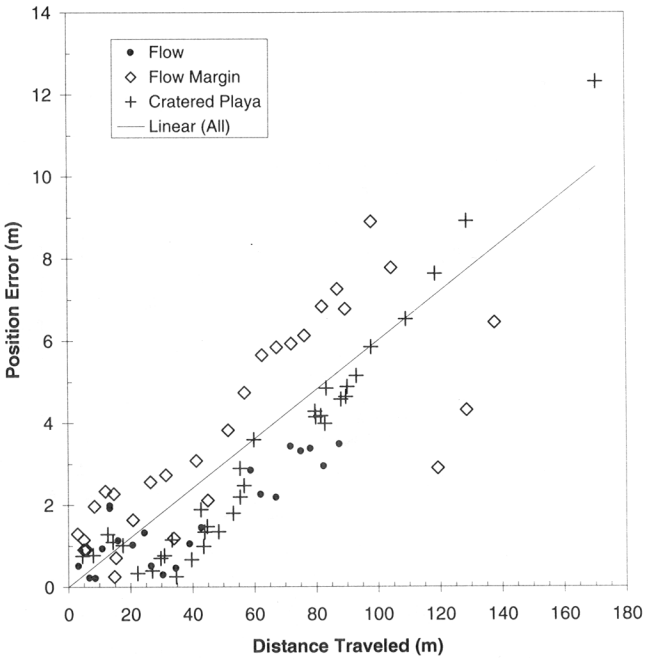

Fig. 8. Plot of all absolute position errors versus respective distance traveled for all field-test traversals. The least-squares fit indicates an expected relative error of 6%.

Experimentation subsequent to these desert-field trials has indicated that the sun sensor was slightly out of calibration during these traverses. This miscalibration added an orientation- and time-dependent bias to the heading of the vehicle, and can account for much of the heading error, which led directly to cross-track error. Figure 10 shows the miscalibrated sun-sensor operation range during the traverse shown in Figure 5b. During the morning (9:30–11:00) the operational area of the sun sensor, due to sun position and rover orientation, caused an error opposite in sign to that of the afternoon (12:00–1:30). Therefore, in the morning, before the turn, the rover drifted to the right—and in the afternoon, after the turn, drifted to the left. Recalibration of the sensor after the field tests removed this problem.

5.3. *Performance Comparison*

Even with the calibration error of the sun sensor, the field tests demonstrated an intrinsic performance improvement

Table 1. Statistical Description of Heading Measurements during Traversals

Traverse	Samples	Std. Dev.	Mean
Sunshine Flow	374	39.5°	−16.7°
Margin before turn	281	6.1°	−7.4°
Margin after turn	188	9.4°	−63.0°
Cratered Playa	500	31.6°	−87.2°

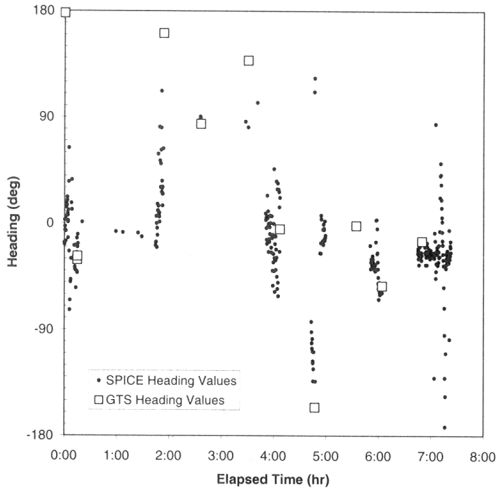

(a) Sunshine flow

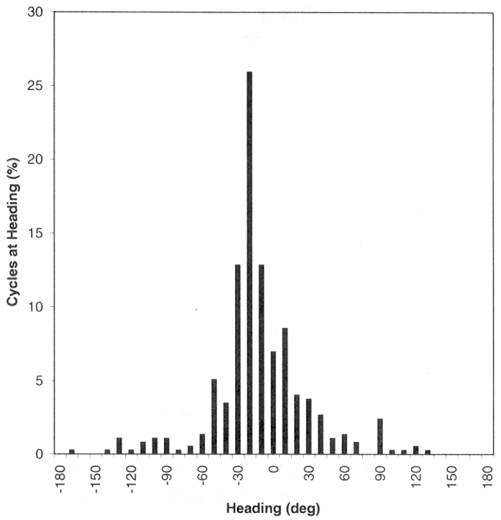

(b) Sunshine flow

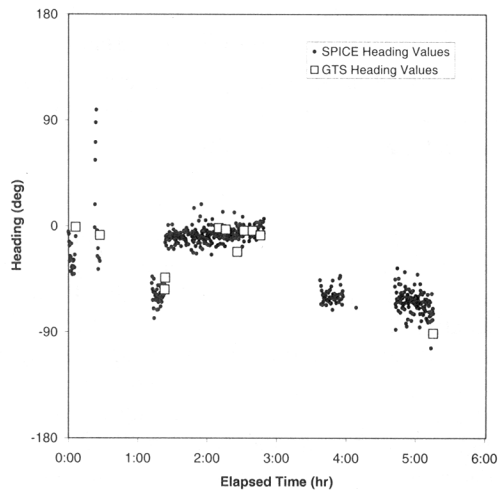

(c) Flow margin

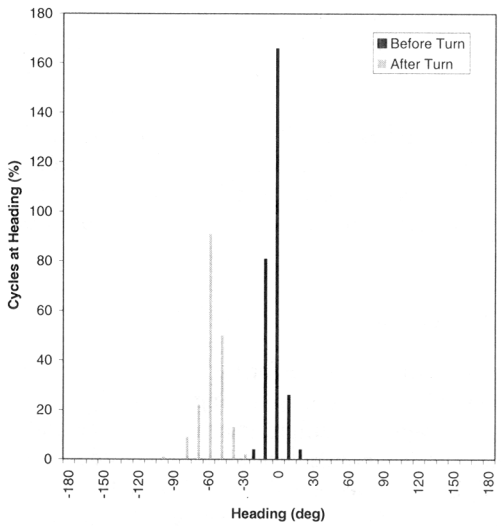

(d) Flow margin

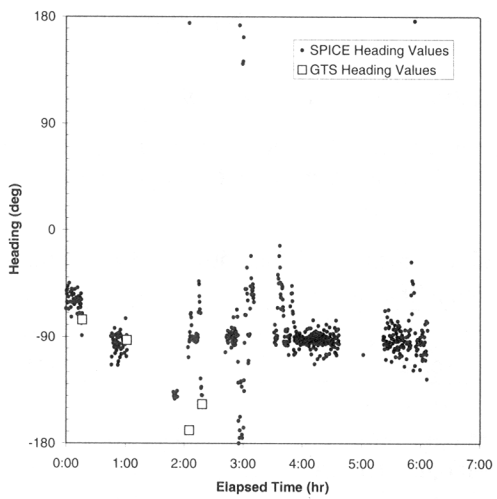

(e) Cratered playa

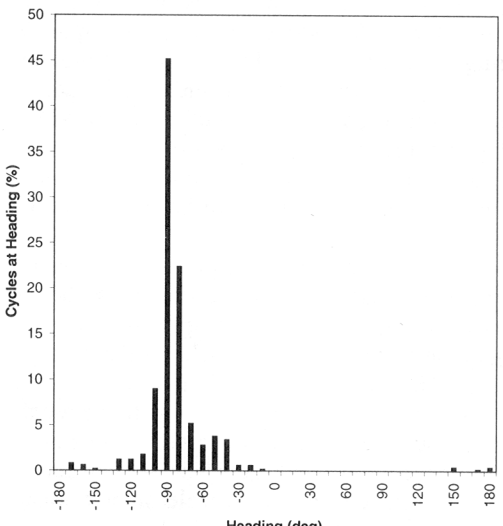

(f) Cratered playa

Fig. 9. Measured heading and distributions during three field-test traversals.

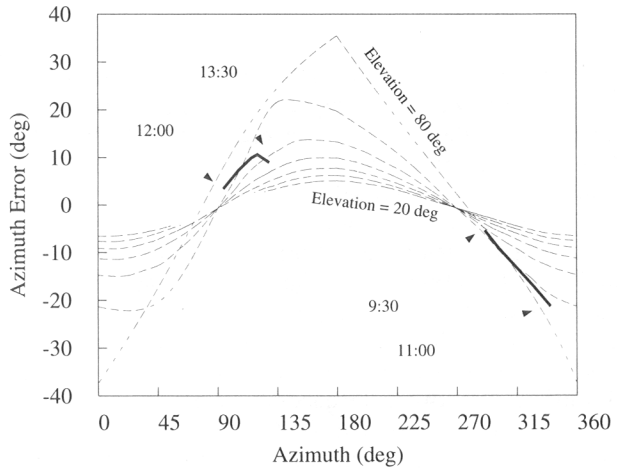

Fig. 10. Plot of sun-sensor azimuth error versus azimuth with different values of elevation shown by contours. This error is due to slight miscalibration of the sun sensor, but can lead to significant errors. See text for details.

when compared with other techniques such as odometry and angular-rate sensing.

5.3.1. Odometry

Odometry-based position and heading estimates of the field-test traverses may be obtained by post-processing the telemetry data. Figure 11 shows the results of using a simple incremental estimation from the data of the traverse in Figure 5b. Figure 11a shows a comparison of the incremental heading obtained from onboard position estimates (SPICE) with that obtained from the independently measured position of the rover (GTS), only for those time values when the independent measurements were available. Also shown are the mean sun-sensor heading and the desired heading to the waypoint.

Since the incremental heading estimate is essentially a derivative of the position, it is an extremely noisy signal. If used instead of a the sun sensor to estimate heading, the propagated estimate of rover position appears as the random walk shown in Figure 11b. This is in strong contrast to the position estimate propagated with the measured heading obtained from the sun sensor, as shown by the solid line in the same plot.

5.3.2. Angular-Rate Sensor

When used in conjunction with odometry, angular-rate sensing provides a moderately useful position estimate, but much poorer than that obtained with sun sensing. This can best be seen by developing a sensor model similar to that provided in Section 5.2.1. In the case of the rate sensor, a bias will

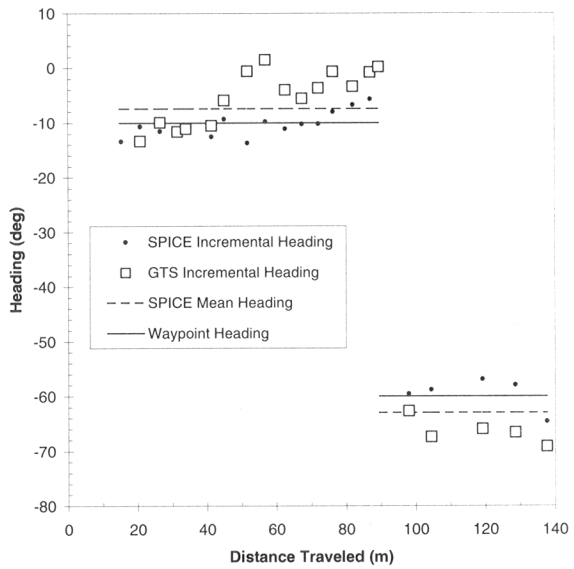

(a) Flow margin

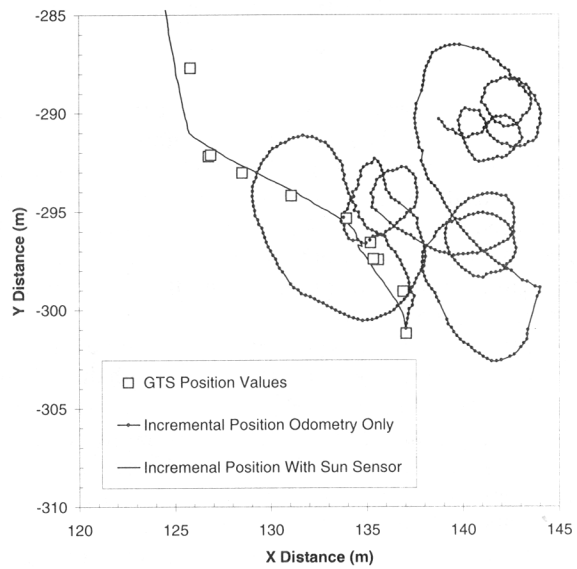

(b) Flow margin

Fig. 11. Comparisons of incremental heading values (a), and position-estimate propagation (b).

typically exist in the rate signal,

$$\theta = \int_0^t (\dot{\theta}_0 + e_\omega)\, d\tau \tag{7}$$

$$= \dot{\theta}_0 t + e_\omega t + \theta_0. \tag{8}$$

Again, for simplicity let $\dot{\theta}_0 = \theta_0 = 0$. Therefore, if the rover speed is v, its (x, y) position will be

$$x = \int_0^t v \cos e_\omega \tau d\tau, \qquad y = \int_0^t v \sin e_\omega \tau d\tau, \tag{9}$$

$$x = \frac{v}{e_\omega} \sin e_\omega t, \qquad y = \frac{v}{e_\omega} (1 - \cos e_\omega t). \tag{10}$$

The straight traverse value of $x = vt = d$ is again used to determine the position error:

$$e_p = \frac{v}{e_\omega} \sqrt{(e_\omega t - \sin e_\omega t)^2 + (1 - \cos e_\omega t)^2}. \tag{11}$$

In the extremes of large and small values for time, this result may be approximated as

$$t \to 0 \; : \quad e_p \approx \frac{e_\omega}{v} \frac{d^2}{2}, \tag{12}$$

$$t \to \infty : \quad e_p \approx d, \tag{13}$$

where the Taylor-series expansion has been used for the first result. For small distances, the error grows with the square of the distance traversed. For intermediate distances, the rate error causes the rover to drift in a circle, and its position error grows precipitously after $e_\omega t = \pi/2$. For large desired distances, the rover will essentially drive in a circle, not making any significant forward progress, and the error will become equal to the traversal distance.

Despite these obvious problems, angular-rate sensors have been used successfully for short traverses with the JPL microrovers *Rocky 3*, in the laboratory, and *Sojourner*, on Mars.[6] To better appreciate *Rocky 7*'s desert-test performance, it can be directly compared with data obtained previously in experiments with *Rocky 3*, and new data from *Sojourner* (Matthies et al. 1995; Wilcox and Nguyen 1998).

Table 2 shows the results for traverses performed by all three rovers. Not only did *Sojourner* have very short average traverse lengths, but its commanded traversals varied greatly from one day of the mission to the next. In contrast, *Rocky 3* was consistently commanded to go a fixed distance in a laboratory setting. Both rovers drove in terrain that was mostly "Mars nominal"; i.e., terrain with a rock-density average for the Martian surface (Moore and Jakosky 1989).

The relative heading error for *Sojourner* is much larger than for *Rocky 3*, as expected by its slow speed. But it is interesting that when vehicle speed is taken into consideration, the rate of heading error is much less for *Sojourner*. This improvement is either due to its space-flight approved electronics, or the reduced vibration noise of low-speed travel under low gravity. Note, however, that changes in the scale of the error do not change its quadratic growth with distance.

The parameter values for heading errors of *Sojourner* and *Rocky 3* have been extracted from the position errors shown in Figure 12. The large variance in the data indicates the noisy quality of rate sensing, but also shows that rate-sensor bias dominates the error. Both plots may be compared with *Rocky 7*'s performance shown in Figure 8, further illustrating the difference between the quadratic rate-sensor error and the linear sun-sensor error. (*Rocky 7* and *Rocky 3* results include intermediate position errors, whereas only end-of-traverse error is known for *Sojourner*.)

To verify that *Rocky 7* error is indeed linear with distance, a quadratic fit was also made to the data shown in Figure 8. The linearity of the data is confirmed by the small relative heading error, provided in parenthesis in Table 2, which is an order of magnitude less than that for *Rocky 3* and *Sojourner*. Without an obvious connection to vehicle speed, this term has not been normalized as a rate of heading error. The use of a quadratic fit actually reduces the size of the absolute heading error to 42 mrad.

Conversely, the quadratic fit to the *Sojourner* and *Rocky 3* data has a substantial linear term, which is provided in Table 2 with parentheses, under absolute heading error. The cause of this term is unknown, but is probably due to slippage. Such an explanation is consistent with slippage being the cause of differences in the relative heading errors obtained for *Rocky 7*, shown above in Figure 7. This linear term for the rate sensor is alone as large as the sun-sensor error. The addition of the quadratic term makes it clear that use of the angular-rate sensor is unsuitable for long-range traversing.

6. Improvements

Even with the improvements provided by sun sensing, plans for 10 km traverse missions across Mars indicate the need to provide even better position estimation. Such information is valuable for scientific understanding of surface features, correlation of ground images with orbital or descent images, and precision-landing rendezvous with the rover for sample return.

Several efforts are under way to improve position estimation of the rover. First, improved calibration of the sun sensor has been performed with a more precise optics model. Second, terrain features and topology are being tracked at multiple resolutions to visually estimate changes in rover position and orientation. Third, local terrain is monitored with the attitude and rocker-bogie sensors to compensate for topological effects. Fourth, improved odometry estimation is being obtained from improved path planning that reduces the total distance traveled and restricts it to the best terrain for driving. Finally, the results of all techniques are being statistically combined onboard the rover (Durrant-Whyte 1986; Balaram 1999).

6. Both used the same sensor: model QRS-11 from Systron Donner.

Table 2. Comparison of Traverse Performance Numbers for *Rocky 7* Using a a Sun Sensor, and *Sojourner* and *Rocky 3*, which Use an Angular-Rate Sensor

	Units	*Rocky 7*	*Sojourner*	*Rocky 3*
Heading sensor		Sun	Rate	Rate
Total odometry (d)	m	395	98	335
Average traverse	m	132	2.1	8.4
Number of traverses		3	46	38
Speed of moves (v)	m/sec	0.12	0.01	0.15
Relative heading error (e_ω/v)	mrad/m	(0.4)	16	5
Rate of heading error (e_ω)	mrad/sec	—	0.16	0.75
Absolute heading error (e_θ)	mrad	60	(105)	(83)
Relative position error (e_p/d)	%	6	—	—

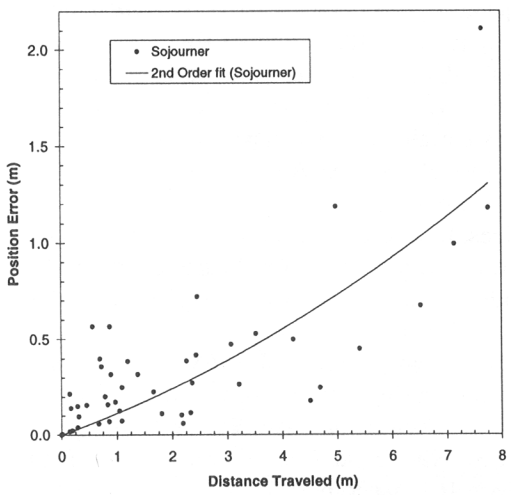

(a) Sojourner drift

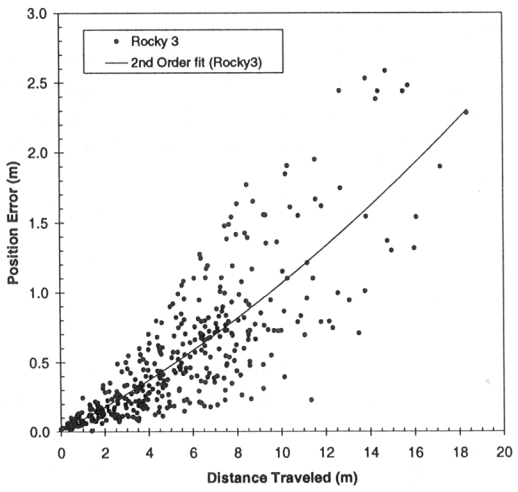

(b) Rocky 3 drift

Fig. 12. Position-error data using angular-rate sensor: for the *Sojourner* rover on Mars (a); and for the *Rocky 3* test vehicle in the laboratory (b).

7. Summary

This paper has presented the results of development and testing of the *Rocky 7* rover prototype, which was created specifically to validate the mission concept of long-range navigation across Mars. To this end, the rover was given the ability to provide panoramic images to remote operators, from which navigation targets were selected and provided back to the rover. Key to *Rocky 7*'s ability to successfully navigate to these sites was precise onboard position estimation (6% relative error), based on sun sensing for heading measurement. Desert-field trials of the rover have validated this operational technique and shown significant improvements over previous direction-sensing schemes.

Acknowledgments

The research described in this paper was carried out by the Jet Propulsion Laboratory, California Institute of Technology, under a contract with the National Aeronautics and Space Administration. Reference herein to any specific commercial product, process, or service by trade name, trademark, manufacturer, or otherwise, does not constitute or imply its endorsement by the United States Government or the Jet Propulsion Laboratory, California Institute of Technology.

In the large experimental systems discussed in this paper there are many individuals contributing. Ground truth data was collected by Curt Niebur and Judd Bowman of Washington University. Data processing within the SPICE system was performed by Boris Semenov. *Rocky 7* telemetry data was captured by Steve Peters. All operations and path specification was performed by Greg Tharp and Ray Arvidson. In addition, the rest of the *Rocky 7* development and field-test team includes: Tim Ohm, J. (Bob) Balaram, Robert Ivlev, Samad Hayati, Paul Backes, Richard Petras, Sharon Laubach, and Alejandro Martin-Alvarez. *Sojourner* performance data was obtained by the Mars *Pathfinder* flight team, and compiled by Tam Nguyen. *Rocky 3* test data was obtained by Reid Harrison and provided by Larry Matthies.

References

Acton, C. 1996. Ancillary data services of NASA's Navigation and Ancillary Information Facility. *Planetary and Space Sci.* 44(1):65–70.

Arvidson, R. E., Acton C., Blaney D., Bowman J., Kim S., Klingelhofer, G., Marshall, J., Niebur, C., Plescia, J., Saunders, R. S., and Ulmer, C. T. 1998. *Rocky 7* prototype Mars rover field geology experiments: 1. Lavic Lake and Sunshine Flow volcanic field, California. *J. Geophys. Res. Planets* 103(EIO):22671–22688.

Backes, P., Tso, K., and Tharp, C. 1998 (May, Leuven, Belgium). Mars *Pathfinder* mission Internet-based operation using WITS. *Proc. of the IEEE Intl. Conf. on Robot. and Automat.* Washington, DC: IEEE.

Balaram, J. Forthcoming. Kinematic state estimation for a Mars rover. *Robotica*, special issue on Intelligent Autonomous Vehicles.

Bickler, D. 1992 (September 28–3O). A new family of JPL planetary surface vehicles. In *Missions, Technologies, and Design of Planetary Mobile Vehicles*. Toulouse, France: Cepadues-Editions, pp. 301–306.

Brooks, R. 1986 (March). A robust layered control system for a mobile robot. *IEEE J. Robot. Automat.* 2(1).

Cozman, F., and Krotkov, E. 1995 (May, Nice, France). Robot localization using a computer vision sextant. *Proc. of the IEEE Intl. Conf. on Robot. and Automat.* Washington, DC: IEEE.

Cozman, F., and Krotkov, E. 1997 (April, Albuquerque, NM). Automatic mountain detection and pose estimation for teleoperation of lunar rovers. *Proc. of the IEEE Intl. Conf. on Robot. and Automat.* Washington, DC: IEEE.

Durrant-Whyte, H. P. 1986 (April). Consistent integration and propagation of disparate sensor observations. *Proc. of the IEEE Intl. Conf. on Robot. and Automat.* Los Alamitos, CA: IEEE, pp. 1464–1469.

Fraden, J. 1993. *AIP Handbook of Modern Sensors: Physics, Designs, and Applications.* New York: American Institute of Physics.

Gat, E., Desai, R., Ivlev, R., Loch, J., and Miller, D. P., 1994. Behavior control for robotic exploration of planetary surfaces. *IEEE Trans. Robot. Automat.* 10(4):490–503.

Matijevic, J., et al. 1997a. Characterization of the Martian surface deposits by the Mars *Pathfinder* rover, *Sojourner. Science* 278(Dec. 5):1765–1768.

Matijevic, J., et al. 1997b. The *Pathfinder* microrover. *J. Geophys. Res.* 102(E2):3989–4001.

Matthies, L., Gat, E., Harrison, R., Wilcox, B., Volpe, R., and Litwin, T. 1995. Mars microrover navigation: Performance evaluation and enhancement. *Autonomous Robots J.*, special issue on Autonomous Vehicles for Planetary Exploration 2(4).

Matthies, L., and Grandjean, P. 1994 (Dec.). Stochastic performance modeling and evaluation of obstacle detectability with imaging range sensors. *IEEE Trans. Robot. Automat.* 10(6):783–791.

Moore, H., and Jakosky, B. 1989. *Viking* landing sites, remote-sensing observations, and physical properties of Martian surface materials. *Icarus* 81:164–184.

Price, S. 1996 (June 27). Microrover sensor-suite design. Phase II Final Report 959855, Lockheed Martin Astronautics, Denver, CO.

Schneider, S., Chen, V., and Pardo-Castellote, G. 1994 (March 20–24, Houston, TX). Controll Shell: A real-time software framework. *NASA Conference Publication 3251, Washington, DCWarrendale, PA: Society of Automotive Engineers.*

Volpe, R. 1998 (June). Sun-sensor heading determination for Mars rover navigation. Internal Engineering Memoran-

dum 3453–98-VO1, Jet Propulsion Laboratory, California Institute of Technology, Pasadena, CA.

Volpe, R., Balaram, 4., Ohm, T., and Ivlev, R. 1996 (November 4–8, Osaka, Japan). The *Rocky 7* Mars rover prototype. *Proc. of the IEEE/RSJ Intl. Conf. on Robots and Sys. (IROS)*. Washington, DC: IEEE.

Volpe, R., Ohm, T., Petras, R., Welch, R., Balaram, J., Ivlev, R. 1997a (Sept. 7–11, Grenoble, France). A prototype manipulation system for Mars rover science operations. *Proc. of the IEEE/RSJ Intl. Conf. on Robots and Sys. (IROS)*. Washington, DC: IEEE.

Volpe, R., Balaram, J., Ohm, T., Ivlev, R. 1997b. *Rocky 7*: A next-generation Mars rover prototype. *J. Adv. Robot.* 11(4):341–358.

Volpe, R., Ohm, T., Petras, R., Welch, R., Balaram, J., Ivlev, R. 1998. Mobile robot manipulators for Mars science. *Space Tech. J.* 17(3/4):219–229.

Wertz, J. (ed.) 1980. *Spacecraft Attitude Determination and Control.* Reidel.

Whittaker, W., Bapna, D., Maimone, M., and Rollins, E. 1997 (July, Tokyo). Atacama desert trek: A planetary analog field experiment. *Proc. of i-SAIRAS Conf.*

Wilcox, B., and Nguyen, T. 1998 (July 13–16, Danvers, MA). *Sojourner* on Mars and lessons learned for future planetary rovers. *Proc. of the Soc. of Automotive Engineers, 28th Intl. Conf. on Environmental Sys. (ICES).*